Mon. Not. R. Astron. Soc. **328,** 71–78 (2001)

ASCA X-ray observations of the disc wind in the dwarf nova Z Camelopardalis

D. S. Baskill,★ P. J. Wheatley and J. P. Osborne
X-Ray Astronomy Group, Department of Physics and Astronomy, Leicester University, Leicester LE1 7RH

Accepted 2001 July 26. Received 2001 July 13; in original form 2000 November

ABSTRACT

We present *ASCA* observations of the dwarf nova Z Camelopardalis during outburst and during a transition from quiescence to another outburst.

At the beginning of the transition the X-ray count rate was an order of magnitude higher and the spectrum much harder than during the outburst. As the transition progressed, the spectrum remained hard as the X-ray flux decreased by a factor of 3, with no spectral softening.

Spectral modelling reveals an optically thin, high-temperature component ($kT \approx 10\,\mathrm{keV}$) which dominates the transition observation and is also observed during outburst. This is expected from material accreting on to the white dwarf surface. The outburst spectra require additional emission at lower temperatures, through either an additional discrete temperature component, or a combination of a cooling flow model and an ionized absorber.

Fits to both observations show large amounts of absorption ($N_{\mathrm{H}} = 8$–$9 \times 10^{21}\,\mathrm{cm}^{-2}$), two orders of magnitude greater than the measured interstellar value, and consistent with UV measurements of the outburst. This suggests that a disc wind is present even in the earliest stages of outburst, possibly before the outburst heating wave has reached the boundary layer.

Key words: stars: dwarf novae – stars: individual: Z Camelopardalis – X-rays: stars.

1 INTRODUCTION

Eclipse observations of dwarf novae during quiescence show that the X-ray-emitting region is centred on the white dwarf, within a size comparable to that of the white dwarf (e.g. HT Cas, Mukai et al. 1997). The emission is believed to originate from material in a boundary layer slowing from a Keplerian velocity in the disc to settle on to the white dwarf surface.

Observations of some systems have shown hard X-ray emission dominating during quiescence and an extreme-ultraviolet component dominating during outburst, when the hard X-ray component is suppressed (Patterson & Raymond 1985a,b; SS Cyg, Cordova et al. 1984; U Gem, Cordova et al. 1980 and Mason et al. 1988; VW Hyi, Pringle et al. 1987). The X-ray flux recovers only at the very end of the optical outburst (Wheatley et al. 1996a).

During quiescence both the accretion rate and the boundary layer density are low, cooling occurs inefficiently, and so the temperature remains high (Pringle & Savonije 1979). During outburst the mass accretion rate increases, the boundary layer becomes optically thick and efficient at cooling, thus the emission of hard X-rays is reduced (Pringle 1977). Such an optically thick boundary layer cools to an effective blackbody temperature of $10^5\,\mathrm{K}$ (10 eV) in the extreme ultraviolet (Patterson & Raymond 1985b).

X-ray observations with the *ROSAT* satellite confirm that this picture also applies to Z Cam during outburst (Wheatley et al. 1996b). However, these *ROSAT* data suffer from the low exposure of the All-Sky Survey, as well as the intrinsic limitations of a soft X-ray proportional counter in the study of hard spectra.

Done & Osborne (1997) have made a detailed analysis of the X-ray spectrum of the dwarf nova SS Cyg using the *Ginga* and *ASCA* satellites. They find that physically plausible spectral fits require models for gas cooling on to the white dwarf surface, with absorption by a photoionized medium. They find that a greater proportion of cool gas and an increase in X-ray reflection is required in outburst than in quiescence.

In this paper we present *ASCA* X-ray spectroscopic observations that caught the dwarf nova Z Cam in outburst in 1995, and observations made during a transition from quiescence to outburst in 1997 (see Fig. 1).

Knigge et al. (1997) observed the same outburst with the Hopkins Ultraviolet Telescope on the *Astro-2* mission. They apply an accretion disc wind model to fit absorption features in the UV spectrum of Z Cam, and conclude that a dense, slow-moving disc wind transition region acts as an absorbing medium with a temperature of a few $\times 10^4$.

★E-mail: dbl@star.le.ac.uk

Modelling of disc winds has been carried out by Proga, Stone & Drew (1998), who find that radiation-driven winds are intrinsically unsteady, with large density and velocity variations. The dense low-velocity flow component of the wind is confined to angles below 45° of the equatorial plane. Z Cam has an inclination of $57 \pm 11°$ (Shafter 1983) and so the line of sight to Z Cam should pass through this zone.

2 OBSERVATIONS

Z Cam has been observed in both outburst and during the optical rise to another outburst using the Japanese *ASCA* satellite. *ASCA* has four X-ray telescopes and detectors: two X-ray CCD cameras (Solid-state Imaging Spectrometers, or SIS) and two gas scintillation imaging proportional counters (Gas Imaging Spectrometers, or GIS) (Tanaka, Inoue & Holt 1994). The SIS detectors have an energy range of 0.4–12 keV whilst the GIS have an energy range of 0.7–15 keV.

As shown in Figs 1 and 2, Z Cam was observed on two occasions: once during outburst over the period 1995 March 8–12 (JD 2449783–2449788), and once during a transition as Z Cam optically brightened to another outburst state on 1997 April 12 (JD 245 0550).

To maximize the number of data, and to avoid unnecessary gaps in the light curve, loose screening criteria have been applied compared with the standard REV2 screening. We reject data from all instruments in both observations when the telescope has deviated more than 0.01° away from the source. The elevation angle between the Earth's limb and satellite pointing direction has been limited to greater than 10° with the SIS and 5° with the GIS, the bright Earth elevation angle is limited to greater than 15° and the radiation background monitor is restricted to less than 250 count s^{-1}. The minimum value of the cut-off rigidity of the geomagnetic field throughout both observations is approximately 4 GeV/c, which is high enough not to require an additional screening criterion. Time filters have been applied to cut out the few remaining periods of very high background during the transitional observation, although this amounts to less than 300 s in all instruments. Circular source extraction regions have been used of 6 arcmin diameter in the GIS and 4 arcmin diameter in the SIS. The background has been taken from the remaining area of the same chip in the SIS, and an annulus of outer radius 18 arcmin around the source for the GIS.

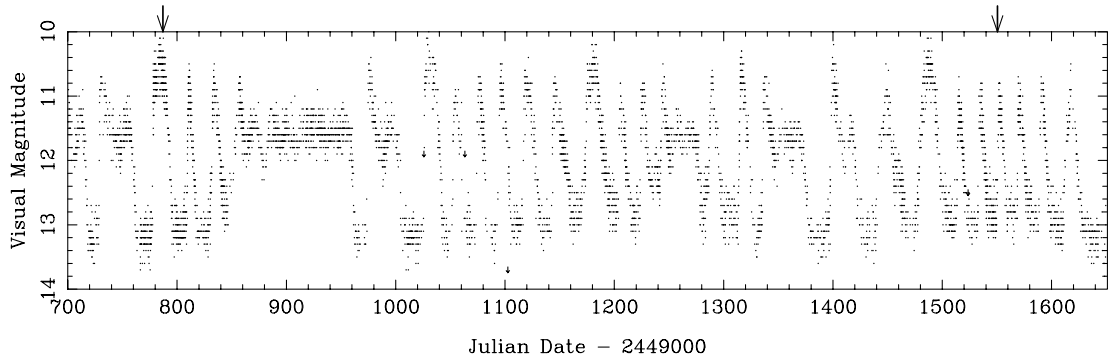

Figure 1. Optical light-curve of Z Cam from AAVSO observations from 1995 January to 1997 July. The times of the *ASCA* observations are shown at JD 244 9783/4 and JD 245 0551.

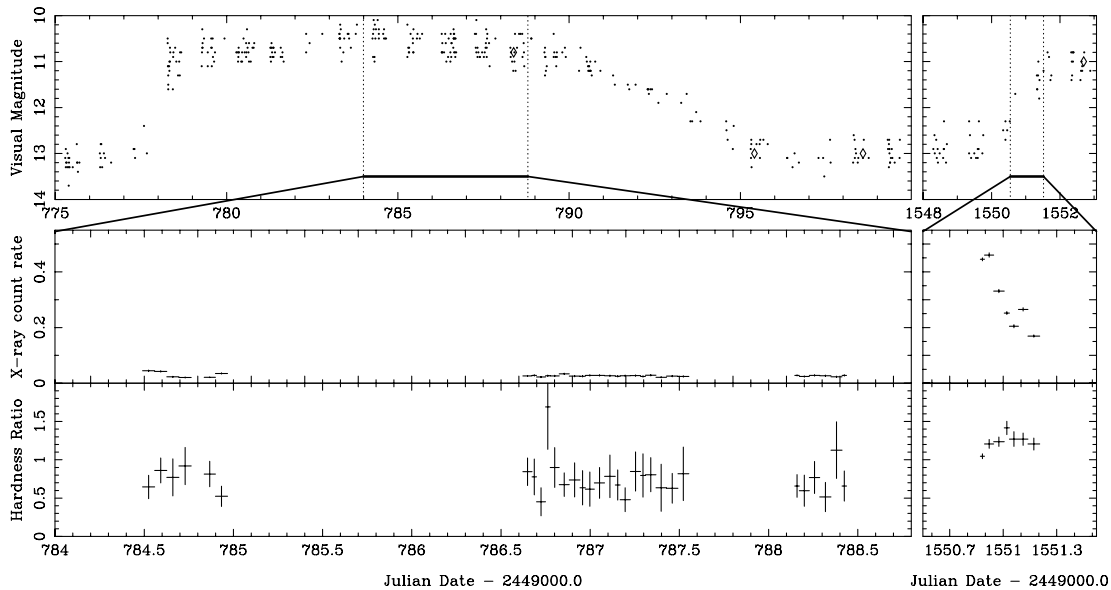

Figure 2. Z Cam in outburst (left) and transition (right) showing the AAVSO visual light curve (top), the ASCA X-ray light curve from all four instruments (middle) and the X-ray hardness ratio (> 2.4 keV light curve divided by the < 2.4 keV light curve) from both GIS instruments.

The outburst observation exposure times after screening are 80 and 76 ks for SIS0 and SIS1 and 94 ks for each GIS. For the transition observation, the exposure times are 18 and 22 ks for the two SIS, and 22 and 23 ks for the two GIS. The response matrices for each SIS have been generated using the FTOOL SISRMG, and for the GIS the standard response matrices (version 0.8, November 1994) have been used. After this loose screening, the two SIS instruments and two GIS instruments were separately combined in both observations. The outburst spectra have been grouped to a minimum of 40 counts per bin and the transition spectra have been grouped to at least 20 counts per bin, allowing χ^2 fitting.

3 LIGHT CURVES

Fig. 2 shows the optical light curve, the X-ray light curve and the X-ray hardness ratio during the two *ASCA* observations. The top panel shows the AAVSO optical observations, and the bottom two panels show the *ASCA* data over a one sixth smaller time range. The hardness ratio shows the plot of the hard light curve (>2.4 keV) over the soft light curve (<2.4 keV). Each bin in Fig. 2 represents one *ASCA* orbit, with each bin defined by gaps in the data arising from Earth occultations and regions of high background.

The optical light curves show that the *ASCA* observations were taken when Z Cam was in an outburst state, and during an optical transition to outburst. Throughout the outburst observation the X-ray count rate was constant, after small initial variations. At the onset of the transition, the X-ray count rate was 20 times the outburst observation count rate. During the transition the X-ray count rate fell dramatically by a factor of 3.

The hardness ratio remained constant throughout the outburst, and was softer than during the optical transition. As the X-ray count rate fell during the transition to outburst, the hardness ratio might have been expected to soften to the level of the earlier outburst observation. However, this is not the case. The hardness ratio appears to increase until midway through the transition, remaining harder than the outburst observation throughout.

Fig. 3 shows the X-ray light curve and hardness ratio of the transitional observation in more detail. The light curve shows a decreasing count rate with irregular peaks. Apart from the large peak in hardness ratio, there appears to be little correlation between the count rate and hardness ratio, with the hardness ratio remaining approximately constant throughout.

4 SPECTRAL ANALYSIS

We selected two pairs of spectra for detailed analysis. These are the SIS and GIS spectra from throughout the outburst and from the entire transition observation.

All the spectra have been fitted with several standard models as used in the XSPEC spectral fitting package, version 11.0 (Arnaud 1996). Throughout the modelling, both SIS and GIS have been fitted simultaneously, with a energy-independent multiplicative factor applied between the SIS and GIS instruments as a free parameter.

4.1 Discrete temperature models

We started the spectral fitting of Z Cam using a single-temperature MEKAL model for emission from a hot diffuse gas (Mewe, Gronenschild & van den Oord 1985; Mewe, Lemen & van den Oord 1986; Liedahl, Osterheld & Goldstein 1995) and WABS to model photoelectric absorption (Morrison & McCammon 1983). This leads to acceptable fits for the transition spectrum ($\chi^2_\nu = 0.77$, 603 degrees of freedom, hereafter d.o.f.) but poor fits to the outburst spectrum ($\chi^2_\nu = 1.72$, 225 d.o.f.). The single temperature fits can be seen in Fig. 4, showing excess emission below 1 keV, especially in the outburst observation.

In an attempt to model the excess emission below 1 keV a second MEKAL component ($kT \approx 0.6$ keV) was added to the model. This component only contributes line emission around 1 keV, predominantly iron L-shell emission, thus resulting in an improved fit. Thus, acceptable fits were obtained to both the outburst and transition spectra (see Table 1).

Not only does this two-temperature model fit both spectra, but also it is only necessary to allow one parameter to vary between the two states, namely the normalization of the higher temperature component ($\chi^2_\nu = 0.71$, 829 d.o.f., fitting both pairs of spectra simultaneously). Thus the spectra of Z Cam can be interpreted as originating from two single-temperature plasmas, with only the amount of hot gas varying between the two observations.

The two-temperature model fits yield large values for the absorption during both the transition ($N_{\rm H} = 11.2^{+1.7}_{-2.4} \times 10^{21}\,{\rm cm}^{-2}$) and the outburst ($N_{\rm H} = 3.1^{+0.4}_{-0.3} \times 10^{21}\,{\rm cm}^{-2}$). The absorption throughout both the outburst and transition is two orders of magnitudes greater than the value of $N_{\rm H} = 4 \times 10^{19}\,{\rm cm}^{-2}$ determined from an *IUE* curve-of-growth study of interstellar absorption lines (C. Mauche, private communication; for method see Mauche, Raymond & Cordova 1988). This excess over the interstellar value suggests that a large amount of absorption is occurring close to the X-ray source, even in the earliest stages of outburst.

As the excess absorption is local to the system, it is unrealistic to expect the absorbing medium to be neutral. Therefore, the neutral absorber was replaced with an ionized absorber in the single temperature MEKAL model. Although this again produces an acceptable fit to the transition spectra ($\chi^2_\nu = 0.67$, 601 d.o.f.) it cannot reproduce the outburst spectra ($\chi^2_\nu = 1.65$, 223 d.o.f.).

4.2 Continuous temperature distribution models

In the previous section we have shown that the data can be modelled with an optically thin plasma at two distinct temperatures. However, the X-rays are expected to originate from only one site, with a continuous range of temperatures representing gas cooling on to the white dwarf.

In an attempt to fit our spectra with a continuous temperature distribution, we adopted the model of Done & Osborne (1997), as applied to the *ASCA* quiescent spectrum of SS Cyg [their *pia*($plT + g$) model]. The model consists of neutral photoelectric absorption to model interstellar absorption (which we freeze at $N_{\rm H} = 4 \times 10^{19}\,{\rm cm}^{-2}$), and an ionized absorption component is required to model absorption local to the system. The emission measure of the X-ray-emitting plasma is modelled as a power law in temperature, $(T/T_{\rm Max})^{\alpha}$ using the CEVMKL model in XSPEC. The *ASCA* observations of Z Cam cannot constrain the reflection continuum component owing to the low number of counts at high energies, and so this has been omitted in our version of the model. However, a Gaussian is included to model the 6.4-keV fluorescent line. We shall refer to this model as the DO97 model hereafter.

The results of the modelling can be seen in Table 2 and Figs 5–9. The metal abundances used throughout are those of Anders & Grevesse (1989), with the abundances frozen at solar values. Thawing the abundances leads to no improvement for the quiescent observation, and marginal improvement to the outburst observation

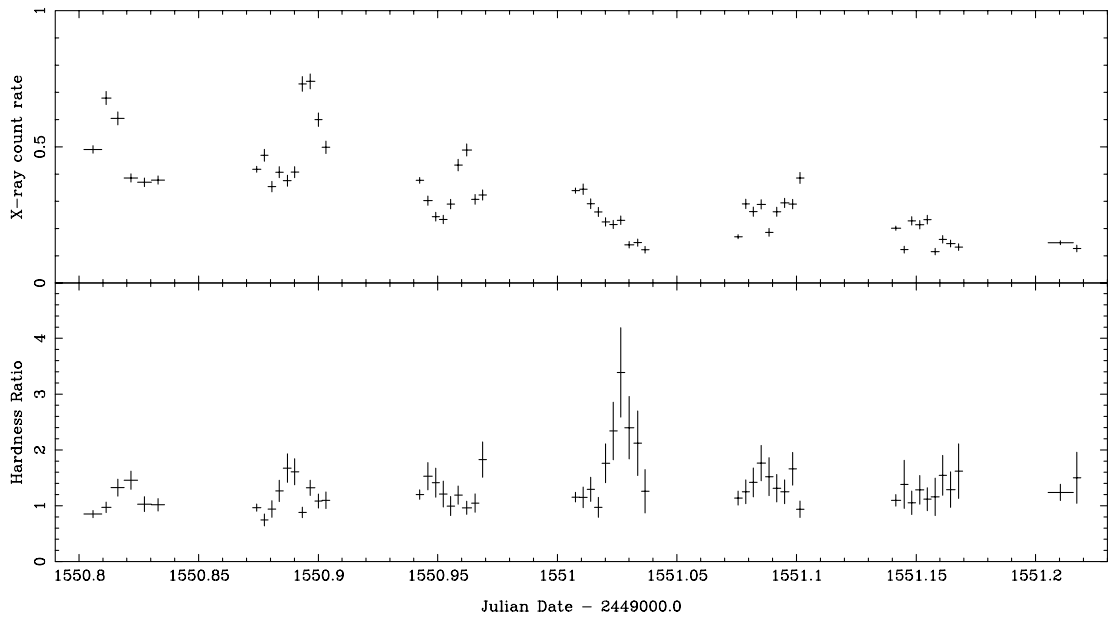

Figure 3. The *ASCA* X-ray light curve from all four instruments (top) and the X-ray hardness ratio (> 2.4 keV light curve divided by the < 2.4 keV light curve) from both GIS instruments (bottom) during the transition observation.

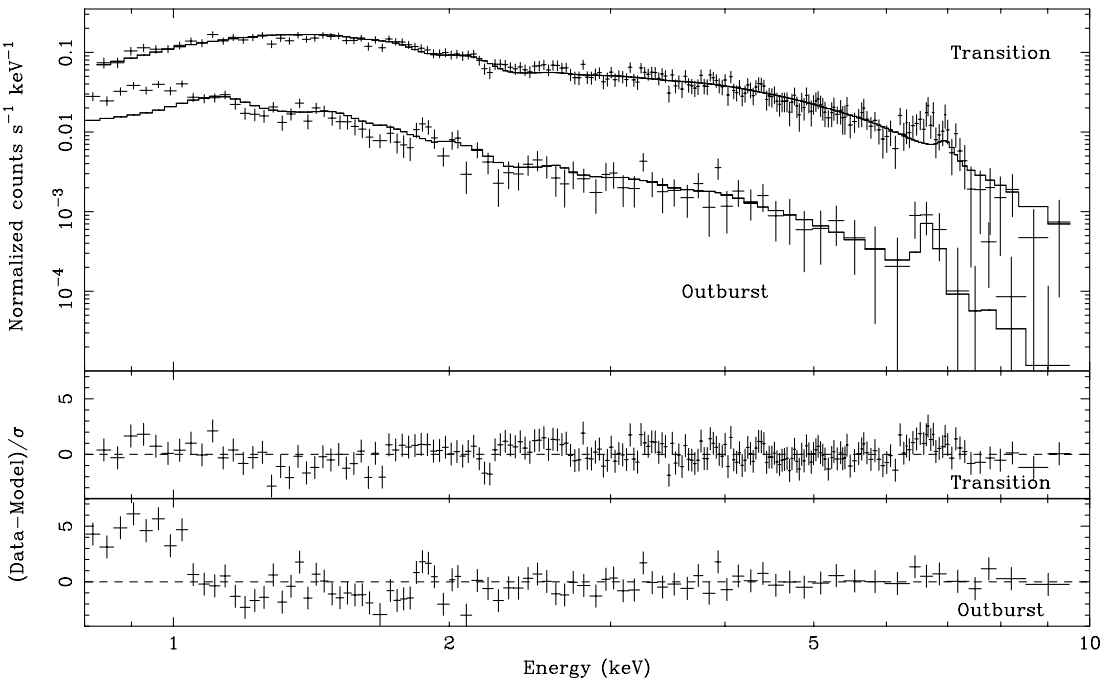

Figure 4. The *ASCA* spectra of the outburst and transition observations, showing the single-temperature model fits. Only the SIS spectra are plotted for clarity. The lower panels show the deviation of the data from the model in units of statistical error, σ.

($\Delta\chi^2 = 3.0$). The maximum temperature of the power-law temperature emissivity component is poorly constrained and so is fixed at 20 keV.

The DO97 model fits as well as the two-temperature model, with $\chi^2_\nu = 0.64$ (600 d.o.f.) during the transition and $\chi^2_\nu = 0.68$ (222 d.o.f.) during outburst. The residuals in the single-temperature fits below 1 keV (Fig. 4) are modelled in the DO97 model by a combination of increased line emission from cool gas and increased absorption. We find that both the ionization state and absorption column of the absorber remain approximately constant, in both the outburst and the transition (see Fig. 8). The power-law emissivity–temperature distribution is weighted towards higher temperature components in the transition observation ($\alpha = 1.6^{+0.5}_{-0.3}$), as would be expected of a cooling flow, and lower temperature components during the outburst ($\alpha = -0.1^{+0.1}_{-0.2}$), which shows an excess of cool gas (see Figs 6 and 7).

To investigate the changing conditions during the transition observation, spectra from both the SIS and GIS have been

Table 1. Results from the two-temperature MEKAL models. The top table shows our best fit to the outburst and transition spectra independently. The lower table shows our best fit to the outburst and transition spectra simultaneously, with just a single parameter free to vary between the two states. All errors are to the 90 per cent confidence level for the single interesting parameter, equivalent to a $\Delta\chi^2$ statistic of 2.706. Normalizations are as implemented in the XSPEC software, in units of $10^{-14}/4\pi d^2 EM$, where EM is the volume emission measure and d is the distance to the source. The bolometric luminosity assumes a distance of 170 pc (Warner 1987).

Component		Transition	Outburst
Equivalent hydrogen column absorption (atom cm^{-2})		$11.2^{+1.7}_{-2.4}\times10^{21}$	$3.1^{+0.4}_{-0.3}\times10^{21}$
Lower temperature:	Temperature (keV)	$0.25^{+0.07}_{-0.05}$	$0.69^{+0.08}_{-0.08}$
	Normalization	$40.6^{+63.2}_{-29.0}\times10^{-3}$	$0.32^{+0.61}_{-0.16}\times10^{-3}$
	Flux (0.8–10.0 keV, erg cm^{-2} s^{-1})	1.3×10^{-12}	0.3×10^{-12}
	Bolometric luminosity (0.1–100.0 keV, erg s^{-1})	0.5×10^{31}	0.1×10^{31}
Higher temperature:	Temperature (keV)	$7.7^{+1.4}_{-1.0}$	$7.5^{+4.0}_{-1.6}$
	Normalization	$14.3^{+0.8}_{-0.8}\times10^{-3}$	$0.59^{+0.04}_{-0.05}\times10^{-3}$
	Flux (0.8–10.0 keV, erg cm^{-2} s^{-1})	2.0×10^{-11}	0.1×10^{-11}
	Bolometric luminosity (0.1–100.0 keV, erg s^{-1})	9.4×10^{31}	0.4×10^{31}
χ^2		398	150
Degrees of freedom		601	223
χ^2_ν		0.66	0.67
Total flux (0.8–10.0 keV, erg cm^{-2} s^{-1})		2.2×10^{-11}	1.3×10^{-12}
Bolometric luminosity (0.1–100.0 keV, erg s^{-1})		9.9×10^{31}	0.6×10^{31}

Component		Transition	Outburst
Equivalent hydrogen column absorption (atom cm^{-2})		$4.8^{+0.4}_{-0.4}\times10^{21}$	
Lower temperature:	Temperature (keV)	$0.65^{+0.03}_{-0.05}$	
	Normalization	$0.59^{+0.09}_{-0.08}\times10^{-3}$	
	Flux (0.8–10.0 keV, erg cm^{-2} s^{-1})	3.9×10^{-13}	
	Bolometric luminosity (0.1–100.0 keV, erg s^{-1})	1.5×10^{30}	
Higher temperature:	Temperature (keV)	$13.9^{+4.0}_{-2.1}$	
	Normalization	$12.2^{+0.3}_{-0.3}\times10^{-3}$	$0.56^{+0.04}_{-0.04}\times10^{-3}$
	Flux (0.8–10.0 keV, erg cm^{-2} s^{-1})	21.1×10^{-12}	0.98×10^{-12}
	Bolometric luminosity (0.1–100.0 keV, erg s^{-1})	1.2×10^{32}	5.7×10^{30}
χ^2			586
Degrees of freedom		829	
χ^2_ν		0.71	
Total flux (0.8–10.0 keV, erg cm^{-2} s^{-1})		21.5×10^{-12}	1.4×10^{-12}
Bolometric luminosity (0.1–100.0 keV, erg s^{-1})		1.2×10^{32}	7.2×10^{30}

temporally divided into seven spectra, with each spectrum fitted with the DO97 model as before. The variation of the *ASCA* count rate, the DO97 best-fitting absorbing material ionization parameter and absorbing $n_{\rm H}$ are shown in Fig. 9. Although there is the indication of variations in both the ionization parameter and the absorbing column, the statistical uncertainties are too large to permit any firm conclusions to be drawn. The temperature variations of the partially ionized absorber are unconstrained and so are not plotted in Fig. 9.

4.3 Flux measurements

Z Cam has previously been observed with both *ROSAT* (Wheatley et al. 1996a) and *EXOSAT* (Mukai & Shiokawa 1993). Our best-fitting DO97 model yields a 0.1–2.5 keV flux of 7.7×10^{-12} erg cm^{-2} s^{-1} in the transition and 1.6×10^{-12} erg cm^{-2} s^{-1} during outburst. These values are a factor of 3 and 6 greater in quiescence and outburst respectively than during the *ROSAT* observations (Wheatley et al. 1996a). Our transition 2–10 keV flux of 2.5×10^{-11} erg cm^{-2} s^{-1} is 50 per cent greater than that measured by *EXOSAT* in quiescence (Wheatley et al. 1996a).

5 DISCUSSION

5.1 Light curves and hardness ratio

The *ASCA* light curves of Z Cam show that the X-ray count rate is greater during the transition to outburst than during outburst, supporting other observations that show X-rays are suppressed during outburst. However, Fig. 2 shows no spectral softening to the outburst level as the transition progresses. During the transition, the optical rise is expected to lead the fall in X-rays, allowing time for the outburst material to travel through to the inner disc. As the material accretes on to the white dwarf surface, the boundary layer becomes optically thick, thus suppressing the hard X-ray emission (Pringle 1977). From Fig. 2 this delay is 0.5–1.5 d, with most of the uncertainty originating from the determination of the beginning of the optical outburst. Therefore, the beginning of the transition observation (from JD 245 0550.79 to JD 245 0551.02) is thought to have been made while the inner disc was still in a quiescent state. The later part of the transition observation may have observed the inner disc of Z Cam in true transition from the quiescent to the outburst state, although there is little difference in the spectra.

Table 2. Our best-fitting DO97 model (see text for details). All errors are to the 90 per cent confidence level ($\Delta\chi^2 = 2.706$). The bolometric luminosity assumes a distance of 170 pc.

Component		Transition	Outburst
Neutral absorber	Absorption $n_{\rm H}$ (atom cm^{-2})	4×10^{19}*	4×10^{19}*
Partially ionized Absorber	Absorption $n_{\rm H}$ (atom cm^{-2})	$9.0^{+1.6}_{-1.5} \times 10^{21}$	$7.8^{+0.4}_{-0.3} \times 10^{21}$
	Temperature (K)	$3.6^{+3.6}_{-3.6} \times 10^{4}$	$4.1^{+6.4}_{-4.1} \times 10^{4}$
	Ionization parameter ξ (L/nR^2, see Done et al. 1992)	$17.8^{+92.1}_{-8.2}$	$8.0^{+67}_{-4.9}$
Continuous temperature emission	power-law index	$1.6^{+0.5}_{-0.3}$	$-0.1^{+0.1}_{-0.2}$
	$T_{\rm max}$ (keV)	20*	20*
	Metal abundance	1.0*	1.0*
	Normalization	$4.0^{+0.9}_{-0.4} \times 10^{-2}$	$5.1^{+1.6}_{-1.4} \times 10^{-4}$
Gaussian	Energy (keV)	6.4*	6.4*
	Equivalent width (eV)	160^{+50}_{-60}	400^{+120}_{-90}
χ^2		386	150
Degrees of freedom		600	222
χ^2_ν		0.64	0.68
Flux (0.8–10.0 keV, erg cm^{-2} s^{-1})		2.2×10^{-11}	0.13×10^{-11}
Bolometric luminosity (0.1–100.0 keV, erg s^{-1})		1.3×10^{32}	9.3×10^{30}

*Parameter frozen at this value.

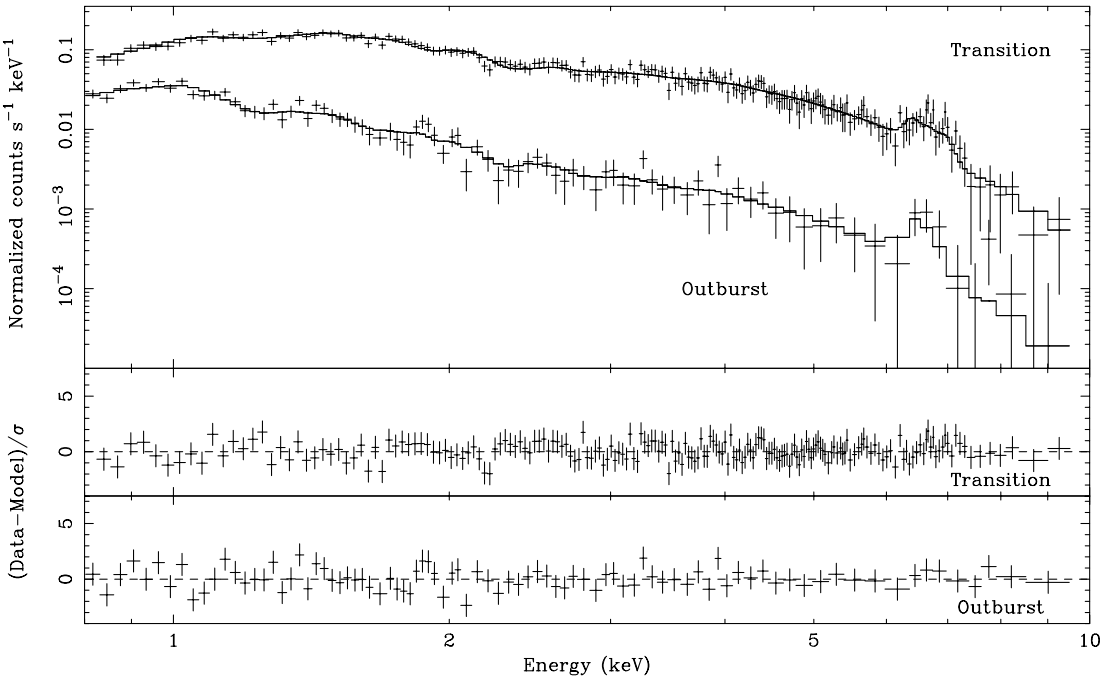

Figure 5. The *ASCA* SIS spectra from the outburst and transition observations, showing our best-fitting DO97 model (see Section 4.2 for details). The lower panels show the deviation of the data from the model in units of statistical error, σ.

5.2 Temperature distribution

We observe high-temperature (≈ 10 keV) emission from the boundary layer in all our model fits, which is reduced during outburst and greater in the transition. Fitting a discrete, two-temperature model to the transition and outburst observations simultaneously yields a remarkable fit with only the normalization of the higher temperature component varying between each state (see Table 1).

Because the flux from the putative cooler component apparently does not vary, we investigate the possibility that the cooler emission may originate from the secondary star, which is expected to emit X-rays from a hot corona. The secondary star of Z Cam is a dwarf of spectral type K7 (Ritter & Kolb 1998), which we assume to be close to the main sequence with a bolometric luminosity of $0.1\,{\rm L}_\odot = 3.8 \times 10^{32}$ erg s^{-1}. The maximum coronal emission from such a star is typically $10^{-3} L_{\rm bol}$ (e.g. Pye et al. 1994; Randich et al. 1996), implying a maximum coronal luminosity for the secondary star in Z Cam of approximately 4×10^{29} erg s^{-1}. In our 'two discrete temperature' modelling, the lower temperature component luminosities are greater than this value ($\gtrsim 10^{30}$ erg s^{-1}). The difference between these two values are not significant enough to rule out the secondary star as the source of the lower temperature component.

Since a continuous distribution of temperatures is more physically reasonable, we consider that this apparent cooler component is probably an artefact of an incorrectly modelled ionized absorber. Therefore, we favour the continuous temperature

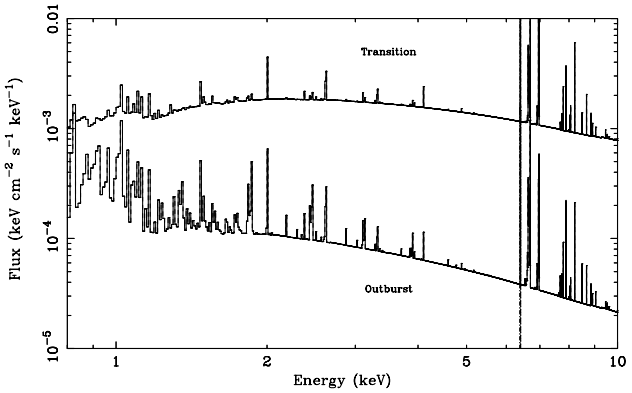

Figure 6. A plot of the incident spectrum for the best-fitting DO97 model, during transition (top) and outburst (bottom).

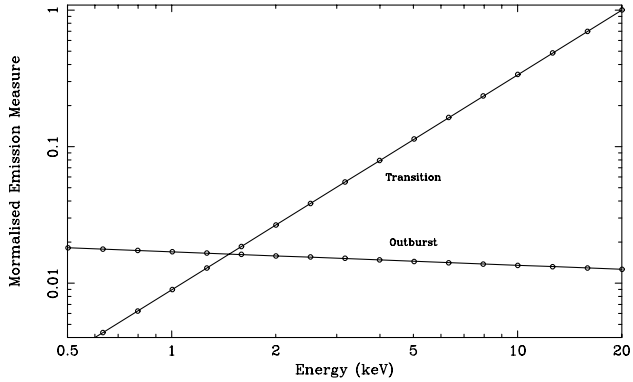

Figure 7. A plot of the differential emission measure for the best-fitting DO97 model during transition and outburst, with a maximum temperature of 20 keV.

distribution DO97 model, which fits the data equally well. The power-law emissivity function is much steeper during the spectrally harder transition than during outburst, as demonstrated in Fig. 2. During the transition the temperature distribution is more like that of a cooling flow, whereas during outburst there is an excess of cool gas. This changing temperature distribution between the transition and outburst has also been observed in *ASCA* observations of SS Cyg (Done & Osborne 1997).

Although it is not possible to constrain the reflected continuum component, the fits require a fluorescent 6.4-keV iron K line, with an equivalent width of 160^{+50}_{-60} eV during the transition (F − statistic = 34.4), and 400^{+120}_{-90} eV during outburst (F-statistic of 6.7, probability > 99.99 per cent). Such a line is a natural consequence of reflection from cool gas.

5.3 Absorption

The DO97 spectral fits suggest that there is absorption beyond interstellar absorption, which is greater by two orders of magnitude in both outburst and the transition. The DO97 model fits suggest that the amount of ionized absorber remains approximately constant throughout both outburst and transition, with $7.8^{+0.4}_{-0.3} \times 10^{21}$ atom cm^{-2} in outburst and $9.0^{+1.6}_{-1.5} \times 10^{21}$ atom cm^{-2} in transition. The level of ionization of the absorbing material remains high in both observations, at 18^{+90}_{-8} in the transition observation to 8^{+67}_{-5} during outburst (errors are to the 90 per cent confidence level, see Fig. 8), and both the ionization parameter and the absorbing column remain high throughout the transition (see Fig. 9). The values of the ionization parameter are consistent with those obtained through studies of SS Cyg ($\xi = 1.4^{+0.3}_{-0.3}$, Done & Osborne 1997).

Knigge et al. (1997) analysed the UV spectrum of Z Cam during the same outburst, and derived the absorption column to be $\approx 10^{22}$ atom cm^{-2} assuming a ionized, solar abundance plasma. They suggested that the absorption in Z Cam is due to a disc wind transition region above and below the accretion disc (cf. Proga et al. 1998). The *ASCA* observations presented in this paper support this, showing that the X-rays produced at the boundary layer were absorbed by the same amount of gas as the ultraviolet photons in both transition and outburst. This suggests that the absorption is associated with vertical structure in the accretion disc, i.e. a clumpy disc wind, and is not associated with the boundary layer.

A disc wind is expected during outburst. However, our analysis indicates that an absorbing wind may also be present early in the transition to outburst (see Figs 8 and 9). Spectral modelling

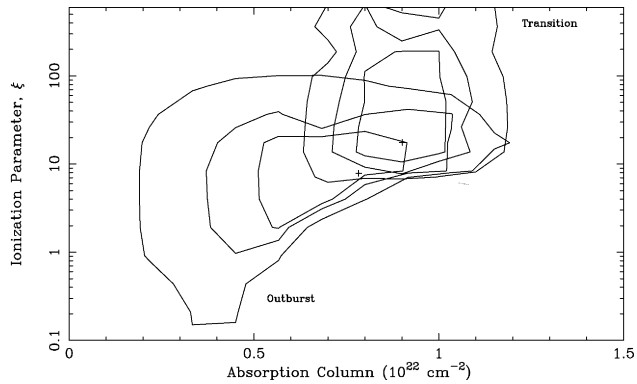

Figure 8. Confidence limits on the ionization parameter ξ and hydrogen column absorption (10^{22} atom cm^{-2}) from the DO97 model fits. The contours represent 68, 95 and 99 per cent confidence limits for the two parameters of interest.

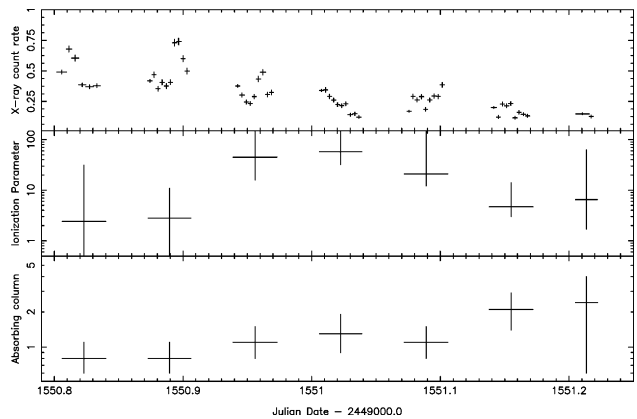

Figure 9. The *ASCA* X-ray light curve (top), the best-fitting DO97 model ionization parameter (ξ in units of L/nR^2, centre) and the best-fitting DO97 model absorbing column ($n_{\rm H}, \times 10^{22}$ atom cm^{-2}, bottom), showing the spectral variations during the transition observation. SIS and GIS spectra have been extracted from each *ASCA* orbit, and fitted simultaneously with the DO97 model as described in the text. Note that both the ionization parameter and the absorbing column are plotted logarithmically. Errors bars in all three panels are 1σ (68.3 per cent confidence level).

suggests that the ionization state of the wind is high during both the outburst and the transition. This implies that the disc wind either starts in the earliest stages of outburst or is present throughout the outburst cycle.

ACKNOWLEDGMENTS

We thank Chris Done, Manabu Ishida, Hajime Inoue, Putra Mahasena and Chris Mauche for useful discussions, and also Chris Mauche for the calculation of the interstellar absorption. We thank the AAVSO for the optical light curves, which are based on observations submitted to the AAVSO by variable star observers worldwide. We also thank the referee, Christian Knigge, for his helpful comments on improving the paper. This research has made use of data obtained from the Leicester Database and Archive Service (LEDAS) at the Department of Physics and Astronomy, Leicester University. DSB acknowledges support of a PPARC studentship (UK) and a two-month Monbusho fellowship (Japan).

REFERENCES

Anders E., Grevesse N., 1989, Geochim. Cosmochim. Acta, 53, 197
Arnaud K. A., 1996, in Jacoby G., Barnes J., eds, ASP Conf. Ser. Vol. 101, Astronomical Data Analysis Software and Systems V. Astron. Soc. Pac., San Francisco, p. 17
Cordova F. A., Chester T. J., Tuohy I. R., Garmire G. P., 1980, ApJ, 235, 163
Cordova F. A., Chester T. J., Mason K. O., Kahn S. M., Garmire G. P., 1984, ApJ, 278, 739
Done C., Osborne J. P., 1997, MNRAS, 288, 649
Knigge C., Long K., Blair B., Wade R., 1997, ApJ, 476, 291
Liedahl D. A., Osterheld A. L., Goldstein W. H., 1995, ApJ, 438, L115
Mason K. O., Cordova F., Watson M. G., King A. R., 1988, MNRAS, 232, 779
Mauche C. W., Raymond J. C., Cordova F. A., 1988, ApJ, 335, 829
Mewe R., Gronenschild E. H. B. M., van den Oord G. H. J., 1985, A&AS, 62, 197
Mewe R., Lemen J. R., van den Oord G. H. J., 1986, A&AS, 65, 511
Morrison R., McCammon D., 1983, ApJ, 270, 119
Mukai K., Shiokawa K., 1993, ApJ, 418, 863
Mukai K., Wood J. H., Naylor T., Schlegel E. M., Swank J. H., 1997, ApJ, 475, 812
Patterson J., Raymond J. C., 1985a, ApJ, 292, 535
Patterson J., Raymond J. C., 1985b, ApJ, 292, 550
Pringle J. E., 1977, MNRAS, 178, 195
Pringle J. E., Savonije G. J., 1979, MNRAS, 187, 777
Pringle J. E. et al., 1987, MNRAS, 225, 73
Proga D., Stone J. M., Drew J. E., 1998, MNRAS, 295, 595
Pye J. P., Hodgkin S. T., Stern R. A., Stauffer J. R., 1994, MNRAS, 266, 798
Randich S., Schmitt J. H. M. M., Prosser C. F., Stauffer J. R., 1996, A&A, 305, 785
Ritter H., Kolb U., 1998, A&AS, 129, 83
Shafter A. W., 1983, PhD thesis, Univ. California at Los Angeles
Tanaka Y., Inoue H., Holt S., 1994, PASJ, 46, 37
Warner B., 1987, MNRAS, 227, 23
Wheatley P. J., van Teeseling A., Watson M. G., Verbunt F., Pfeffermann E., 1996a, MNRAS, 283, 101
Wheatley P. J., Verbunt F., Belloni T., Watson M. G., Naylor T., Ishida M., Duck S. R., Pfeffermann E., 1996b, A&A, 307, 137

This paper has been typeset from a TEX/LATEX file prepared by the author.